Quantifying the nitrogen equilibrium and photochemistry-induced isotopic effects between NO and NO$_2$

Jianghanyang Li[1], Xuan Zhang[2], Greg Michalski[1,3], John Orlando[2], and Geoffrey Tyndall[2]

[1.] Department of Earth, Atmospheric and Planetary Sciences, Purdue University, West Lafayette, IN, 47907

[2.] Atmospheric Chemistry Observations and Modeling Lab, National Center for Atmospheric Research, Boulder, CO, 80301

[3.] Department of Chemistry, Purdue University, West Lafayette, IN, 47907

Correspondence to: Jianghanyang Li (li2502@purdue.edu)

Abstract. The nitrogen isotopic fractionations between NO and NO$_2$ play a significant role in determining the nitrogen isotopic compositions (δ^{15}N) of atmospheric NO$_2$ and nitrate. This isotopic fractionation is controlled by a combination of equilibrium isotopic effect (EIE) and Leighton Cycle induced isotopic effect (LCIE), which are poorly constrained. We quantified this isotopic fractionation process by 1) measuring the isotopic fractionation factors of EIE and LCIE in a 10 m^3 atmospheric simulation chamber and 2) mathematically calculating the relative importance of EIE and LCIE. Our results showed the enrichment factors of EIE and LCIE are 1.0275±0.0012, and 0.990±0.005, respectively, at room temperature. We find that EIE is the dominate factor when NO$_x$ >20 nmol mol^{-1}, and LCIE is more important at low NO$_x$ concentrations (<1 nmol mol^{-1}) and high rates of photolysis of NO$_2$ (j(NO$_2$)). Our study provides a mathematical solution to calculate the NO-NO$_2$ isotopic fractionation at any given condition.

Atmospheric
Chemistry
and Physics

Discussions

Open Access

1. Introduction

24

25   The variation in the nitrogen isotopic composition ($\delta^{15}N$) of NO_2 and nitrate is an important

26   tool in understanding the sources and chemistry of atmospheric NO_x ($NO+NO_2$). Atmospheric

27    $NO_{2(g)}$, nitrate aerosols, and nitrate ion in the precipitation imprint the $\delta^{15}N$ of their sources (Elliott

28   et al., 2009; Kendall et al., 2007) thus many studies have used the $\delta^{15}N$ values of atmospheric

29    $NO_{2(g)}$ or nitrate to investigate NO_x sources (Chang et al., 2018; Felix et al., 2012; Felix & Elliott,

30   2014; Gobel et al., 2013; Hastings et al., 2004, 2009; Morin et al., 2009; Park et al., 2018; Walters

31   et al., 2015, 2018). However, there remain questions about how isotopic fractionations occurring

32   during photochemical recycling of NO_x and its conversion into NO_y (NO_3, N_2O_5, HONO, etc.) and

33   nitrate alter the $\delta^{15}N$ values of NO_x (Chang et al., 2018; Freyer, 1991; Hastings et al., 2004; Jarvis

34   et al., 2008; Michalski et al., 2005; Morin et al., 2009; Zong et al., 2017). Isotopic fractionations

35   occur in most, if not all, NO_x and NO_y reactions. However, most isotopic fractionation factors

36   related to NO_x and NO_y chemistry are still unknown. In addition, since the atmospheric chemistry

37   of NO_x varies significantly in different environments (e.g., polluted vs. pristine, night vs. noon),

38   the isotopic fractionations associated with the chemistry are also likely to vary under different

39   environments. These uncertainties could potentially bias conclusions reached on NO_x source

40   apportionment using nitrogen isotopes. Therefore, a better quantification of these isotopic

41   fractionations is needed. The isotopic fractionations between NO and NO_2 have been suggested to

42   be the dominant factor in determining the $\delta^{15}N$ of NO_2 and ultimately nitrate (Freyer, 1991; Freyer

43   et al., 1993; Savarino et al., 2013; Walters et al., 2016), therefore understanding the isotopic

44   fractionations between NO and NO_2 could improve our understanding on the isotopes of

45   atmospheric NO_2 and nitrate.

46   In general, there are three types of isotope fractionation effects associated with NO_x

47   chemistry: 1) the equilibrium isotopic effect (EIE), i.e., isotopic exchange between two compounds

48   without forming new molecules (Freyer et al., 1993; Walters et al., 2016), for nitrogen isotopes in

49   the NO_x system this is the $^{15}NO + {}^{14}NO_2 \leftrightarrow {}^{14}NO + {}^{15}NO_2$ exchange reaction; 2) the kinetic isotopic

50   effect (KIE) associated with difference in isotopologue rate coefficients during unidirectional

51   reactions (Bigeleisen & Wolfsberg, 1957), in the NO_x system these could be manifest in the

52   oxidation of NO into NO_2 by $O_3/HO_2/RO_2$; 3) the photochemical isotopic fractionation effect

53   (PHIFE, Michalski et al., 2004; Miller & Yung, 2000), which for NO_x is the isotopic fractionation

54   associated with NO_2 photolysis. All three fractionations impact the $\delta^{15}N$ value of NO_2 and

55   consequently nitrate but the relative importance of each may vary. Additionally, in the NO_y cycle,

56   EIE (isotopic exchange between NO_2, NO_3 and N_2O_5), KIE (formation of NO_3, N_2O_5 and nitrate)

57   and PHIFE (photolysis of NO_3, N_2O_5, HONO and sometimes nitrate) may also exist and be

58   relevant for the $\delta^{15}N$ of HNO_3 and HONO, but these will not be discussed in this work.

59   The isotopic fractionation factors of EIE, KIE and PHIFE in the NO_x cycle still have

60   significant uncertainties. Discrepancies in the EIE for $^{15}NO + NO_2 \leftrightarrow NO + {}^{15}NO_2$ have been noted

61   in several studies. Theoretical calculations predict fractionation factors (α) ranging from 1.035 to

62   1.042 at room temperature (Begun & Fletcher, 1960; Monse et al., 1969; Walters & Michalski,

63   2015). In contrast two separate experiments measured slightly different fractionation factors of

64   1.028±0.002 (Begun & Melton, 1956) and 1.0356±0.001 (Walters et al., 2016). A concern in both

65   experiments is that they were conducted in chambers with extremely high NO_x concentrations

66   (hundreds of µmol mol^{-1}) that were significantly higher than typical ambient atmospheric NO_x

67   levels (usually <100 nmol mol^{-1}). Whether the isotopic fractionation factors determined by these

68   experiments are applicable in the ambient environment is uncertain. KIE and PHIFE have been

69   rarely studied theoretically or experimentally and were often overlooked. Freyer et al. (1993)

70   suggested that the NO_x photochemical cycle (KIE and PHIFE) tends to diminish the equilibrium

71   isotopic fractionation (EIE) between NO and NO_2 if it assumed that the isotopic fractionation

72   factors of KIE and PHIFE are both 1. Alternatively, Freyer et al. (1993) estimated the isotopic

73   fractionation factor between NO and NO_2 at Julich, Germany over a 1-year period which averaged

74   at 1.018±0.001 and suggested that this fractionation factor was a combined effect of EIE, KIE and

75   PHIFE. Even if this approach were valid, applying this single fractionation factor elsewhere, where

76   NO_x, O_3 concentrations and actinic fluxes are likely different, would be tenuous given that these

77   factors may influence the relative importance of EIE, KIE and PHIFE (Hastings et al., 2004;

78   Walters et al., 2016). Therefore, to quantify the overall isotopic fractionations between NO and

79   NO_2 at any given condition, it is crucial to know 1) isotopic fractionation factors of EIE, KIE and

80   PHIFE individually and 2) the relative importance of each factor in various conditions.

81   In this work, we aim to quantify the nitrogen isotopic fractionation between NO and NO_2

82   at photochemical equilibrium. First, we measure the isotopic fractionations between NO and NO_2

83   in an atmospheric simulation chamber at atmospheric relevant NO_x levels. Then, we provide

84   mathematical solutions to assess the impact of NO_x level and NO_2 photolysis rate (j(NO_2)) to the

85   relative importance of EIE, KIE and PHIFE. Subsequently we use the solutions and chamber

86   measurements to calculate the isotopic fractionation factors of EIE, KIE and PHIFE. Last, using

87   the calculated fractionation factors and the equations, we model the NO-NO_2 isotopic

88   fractionations at several sites to illustrate the behavior of NO_x nitrogen isotopes in the ambient

89   environment.

90

91   **2. Methods**

92   The experiments were conducted using a 10 m^3 Atmospheric Simulation Chamber at the

93   National Center for Atmospheric Research (see descriptions in supplementary material and Zhang

94   et al. (2018)). A set of mass flow controllers was used to inject NO and O_3 into the chamber: NO

95   was injected at 1 L min^{-1} from an in-house concentrated NO cylinder (133.16 µmol mol^{-1} NO in

96   ultra-pure N_2), and O_3 was generated by flowing 5 L min^{-1} zero-air through a flow tube equipped

97   with a Pen-Ray lamp (UVP LLC., CA) into the chamber. The wall loss rate of NO_2 was tested and

98   found to be negligible (see supplementary material). In each experiment, the actual amounts of

99   NO and O_3 injected were calculated using measured NO_x and O_3 concentrations after steady state

100   was reached (usually within 1 h).

101   Two sets of experiments were conducted to separately investigate the EIE, KIE and PHIFE.

102   The first set of experiments was conducted in the dark. In each experiment, a range of NO and O_3

103   ([O_3]<[NO]) was injected into the chamber to produce NO-NO_2 mixtures. The N isotopes of these

104   mixtures were used to investigate the EIE between NO and NO_2. The second set of experiments

105   was conducted under irradiation of UV lights. Under such conditions, NO, NO_2 and O_3 reached

106   photochemical steady state, which revealed the combined isotopic effects of EIE, KIE and PHIFE.

107   In addition, the $\delta^{15}N$ value of source NO was measured throughout the experiments. For each test,

108   a certain amount of O_3 was injected into the chamber, then approximately the same amount of NO

109   was injected into the chamber to ensure all the NO_x was in the form of NO_2 with little O_3 (<3 nmol

110   mol^{-1}) remaining in the chamber such that the O_3+NO_2 reaction was negligible, the $\delta^{15}N$ value of

111   NO_2 therefore represented the $\delta^{15}N$ of source NO.

112   During each experiment, once the concentrations of NO, NO_2 and O_3 reached steady state,

113   NO_2 was collected from the chamber onto a honeycomb denuder tube as NO_2^- while NO was inert

114   to the chemicals on the denuder tubes. The NO_2 collection efficiency of a single honeycomb

Atmospheric
Chemistry
and Physics
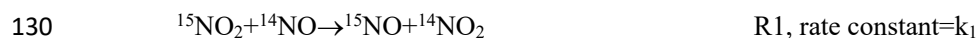Discussions
Open Access
EGU

115 denuder tube was tested to be nearly 100% (see supplementary material). Each denuder tube was

116 then rinsed thoroughly with 10 ml deionized water into a clean polypropylene centrifuge tube and

117 stored frozen until isotopic analysis. Isotopic analysis was conducted at Purdue Stable Isotope

118 Laboratory. For each sample, approximately 50 nmol of NO_2^- was mixed with 2 M sodium azide

119 solution in acetic acid buffer in an air-tight glass vial, then shaken overnight to completely reduce

120 all the NO_2^- to $N_2O_{(g)}$ (Casciotti & McIlvin, 2007; McIlvin & Altabet, 2005). The product N_2O

121 was directed into a Finnigan GasBench equipped with cryo-trap then the $\delta^{15}N$ of the N_2O was

122 measured by a Delta-V Isotope Ratios Mass Spectrometer (IRMS). The overall analytical

123 uncertainty for $\delta^{15}N$ analysis was ±0.5 ‰ (1σ) based on replicate analysis of in house NO_2^-

124 standards.

125

126 **3. Results and Discussions**

127 **3.1. Equilibrium Isotopic Fractionation between NO and NO_2**

128   The equilibrium isotopic fractionation factor α(NO_2-NO) is the ^{15}N enrichment in NO_2

129 relative to NO, and is expressed as the difference in rate constants between the two reactions:

130      $^{15}NO_2 + ^{14}NO \rightarrow ^{15}NO + ^{14}NO_2$ R1, rate constant=k_1

131      $^{15}NO + ^{14}NO_2 \rightarrow ^{15}NO_2 + ^{14}NO$ R2, rate constant=$k_1 \times$α(NO_2-NO)

132 where k_1 is the rate constant of the isotopic exchange, which was previously determined to be

133 8.14×10^{-14} cm^3 s^{-1} (Sharma et al., 1970). The reaction time for NO-NO_2 to reach isotopic

134 equilibrium was estimated using a simple box model containing N isotopic information (see

135 supplementary information). At the NO_x level during the chamber experiments (7.7-62.4 nmol

136 mol^{-1}), the isotopic equilibrium was reached within 15 min, and the sample collection usually

Atmospheric
Chemistry
and Physics
Discussions

137   started 1 hour after NO_x was well mixed in the chamber. The isotope equilibrium fractionation

138   factor is then calculated to be:

139    $$\alpha(NO_2 - NO) = \frac{[^{15}NO_2] \times [^{14}NO]}{[^{14}NO_2] \times [^{15}NO]} = \frac{R(NO_2)}{R(NO)}$$ Eq. (1)

140   where R(NO, NO_2) are the $^{15}N/^{14}N$ ratios of $NO_{1,2}$. As $\delta(^{15}N, NO) = (R(NO)/R(reference)-1) \times 1000$ ‰

141   and $\delta(^{15}N, NO_2) = (R(NO_2)/R(reference)-1) \times 1000$ ‰ (hereafter, the $\delta^{15}N$ values of NO, NO_2 and

142   NO_x are referred as $\delta(NO)$, $\delta(NO_2)$ and $\delta(NO_x)$, respectively), Eq. (1) leads to:

143    $$\delta(NO_2) - \delta(NO) = (\alpha(NO_2 - NO) - 1) \times 1000\ ‰ \times (1 + \delta(NO))$$

144    $$= \varepsilon(NO_2 - NO) \times (1 + \delta(NO))$$ Eq. (2)

145   where $\varepsilon(NO_2\text{-}NO)$ is the isotope enrichment factor (in permil (‰), Hoefs, 2009). Combining Eq.

146   (2) with the NO_x isotopic mass balance $(\delta(NO_x) = f(NO_2) \times \delta(NO_2) + (1-f(NO_2)) \times \delta(NO)$,

147    $f(NO_2) = [NO_2]/([NO] + [NO_2]))$ yields:

148    $$\delta(NO_2) - \delta(NO_x) = \varepsilon(NO_2 - NO) \times (1 + \varepsilon(NO_2 - NO)) \times (1 + \delta(NO_2)) \times (1 - f(NO_2))$$ Eq. (3)

149   In which $\delta(NO_x)$ equals to the $\delta^{15}N$ of source NO, and $f(NO_2)$ is the molar fraction of NO_2. Three

150   calibration experiments that measured $\delta(NO_x)$ before, during and after all the experiments showed

151   consistent $\delta(NO_x)$ values of -58.7±0.8 ‰ (n = 3), indicating $\delta(NO_x)$ remained unchanged

152   throughout the experiments. Thus, the $\delta(NO_x)$ can be treated as a constant in Eq. (3), and the slope

153   of a linear regression of $(\delta(NO_2)\text{-}\delta(NO_x))/(1+\delta(NO_2))$ versus $1\text{-}f(NO_2)$ represents $\varepsilon(NO_2\text{-}$

154    $NO)/(1+\varepsilon(NO_2\text{-}NO))$.

155   The plot of $(\delta(NO_2)\text{-}\delta(NO_x))/(1+\delta(NO_2))$ as a function of $1\text{-}f(NO_2)$ values from five

156   experiments yields a slope of +26.8±1.2 ‰ (Fig. 1A) therefore an $\varepsilon(NO_2\text{-}NO)$ of 27.5±1.2 ‰ at

157   room temperature. This fractionation factor was comparable to previously measured values with

158   some differences. Our result agrees well with the $\alpha(NO_2\text{-}NO)$ value of 1.028±0.002 obtained by

159   Begun and Melton (1956) at room temperature. However, Walters et al., (2016) determined the

160    $\alpha(NO_2\text{-}NO)$ values of NO-NO$_2$ exchange in a 1-liter reaction vessel, which showed a slightly

161   higher $\alpha(NO_2\text{-}NO)$ value of 1.035. This discrepancy likely originates from rapid heterogeneous

162   reactions on the wall of the reaction vessel at high NO$_x$ concentrations in Walters et al.

163   (2016).Walters et al. (2016) used a vacuum line and Pyrex reaction vessel, which are known to

164   absorb water (Do Remus et al., 1983; Takei et al., 1997) that can react with NO$_2$ forming HONO,

165   HNO$_3$ and other species. Additionally, previous studies have suggested that glass walls could

166   enhance the formation rate of N$_2$O$_4$ by over an order of magnitude (Barney & Finlayson-Pitts,

167   2000; Saliba et al., 2001). At isotopic equilibrium, N$_2$O$_4$ is enriched in ^{15}N compared to NO and

168   NO$_2$ (Walters & Michalski, 2015). Therefore, their measured $\alpha(NO_2\text{-}NO)$ might be slightly higher

169   than the actual $\alpha(NO_2\text{-}NO)$ value. In this work, the chamber wall was made of Teflon, which

170   showed minimum NO$_2$ wall reactions and the low NO$_x$ mixing ratio minimized N$_2$O$_4$ formation.

171   Therefore, we suggest our measured $\alpha(NO_2\text{-}NO)$ value (1.0275±0.0012) should better reflect the

172   NO-NO$_2$ EIE in the atmosphere.

173   **3.2. Kinetic isotopic fractionation of Leighton Cycle**

174   The photochemical reactions of NO$_x$ complicate the isotopic fractionations between NO

175   and NO$_2$. Since there were no VOCs or OH sources in the chamber (the photolysis of O$_3$ as the

176   OH precursor is minor at the wavelength of blacklights used in the chamber), the formation of RO$_2$

177   and HO$_2$ can be neglected, and the NO-NO$_2$ photochemistry cycle in the chamber was controlled

178   by NO$_2$ photolysis and the NO + O$_3$ reaction. Hence the KIE (R3-R4) and the PHIFE in R5-R6

179   were competing with the EIE between NO and NO$_2$ (R1-R2):

180    $^{14}NO_2 \rightarrow {}^{14}NO + O$ R3, rate constant=j(NO$_2$)

181    $^{15}NO_2 \rightarrow {}^{15}NO + O$ R4, rate constant=j(NO$_2$)×α_1

182 $\quad$ $^{14}NO + O_3 \rightarrow {}^{14}NO_2 + O_2$ $\qquad$ R5, rate constant=k_5

183 $\quad$ $^{15}NO + O_3 \rightarrow {}^{15}NO_2 + O_2$ $\qquad$ R6, rate constant=$k_5 \times \alpha_2$

184 In which $j(NO_2)$ is the NO_2 photolysis rate (1.4×10^{-3} s^{-1} in the experiments), k_5 is the rate constant

185 for the $NO + O_3$ reaction (1.73×10^{-14} cm^3 s^{-1}, Atkinson et al., 2004), and $\alpha_{1,2}$ are isotopic

186 fractionation factors of the two reactions. Previous studies (Freyer et al., 1993; Walters et al., 2016)

187 have attempted to assess the competition between EIE (R1-R2), KIE and PHIFE (R3-R6), but none

188 of them quantified the relative importance of the two processes, nor were α_1 or α_2 values

189 determined. Here we provide the mathematical solution of EIE, KIE and PHIFE to illustrate how

190 R1-R6 affect the isotopic fractionations between NO and NO_2.

191 $\qquad$ To demonstrate the competition between R1-R2 and R3-R6, we define:

192 $\quad$
$$A = \begin{cases} \dfrac{\tau_{exchange}}{\tau_{photo}} & \text{when } j(NO_2) \neq 0 \\ \\ 0 & \text{when } j(NO_2) = 0 \end{cases}$$
Eq. (4)

193 in which $\tau_{exchange}$ is the NO_2 lifetime with respect to isotopic exchange with NO and τ_{photo} is the

194 NO_2 lifetime with respect to photolysis:

195 $\quad$ $\tau_{exchange} = \dfrac{1}{k_1 \times [NO]}$ $\qquad$ Eq. (5)

196 $\quad$ $\tau_{photo} = \dfrac{1}{j(NO_2)}$

197 $\qquad$ Eq. (6)

198 The expression for A, R1-R6 and Eq. (1)-(6) were used to derive the $\delta(NO_2)$-$\delta(NO)$ and $\delta(NO_2)$-

199 $\delta(NO_x)$ values at steady state (see calculation in supplementary material):

200 $\quad$ $\delta(NO_2) - \delta(NO) \ (\text{‰}) = \dfrac{(\alpha_2 - \alpha_1) \times A + (\alpha(NO_2 - NO) - 1)}{A + 1} \times 1000 \ \text{‰}$ $\qquad$ Eq. (7)

201 $\quad$ $\delta(NO_2) - \delta(NO_x) \ (\text{‰}) = \dfrac{(\alpha_2 - \alpha_1) \times A + (\alpha(NO_2 - NO) - 1)}{A + 1} \times (1 - f(NO_2)) \times 1000 \ \text{‰}$ $\qquad$ Eq. (8)

202 Equation (7) shows the isotopic fractionation between NO and NO_2 ($\delta(NO_2)$-$\delta(NO)$) is determined

203 by A, the EIE factor ($\alpha(NO_2$-NO)-1) and the (α_2-α_1) factor. This (α_2-α_1) factor represents a

204 combination of KIE and PHIFE, suggesting they act together as one factor; therefore, we name the

205 (α_2-α_1) factor LCIE (Leighton Cycle Isotopic Effect). Using measured $\delta(NO_2)$-$\delta(NO)$ values, A

206 values, and the previously determined EIE factor, we calculated that the best fit for the LCIE factor

207 was -10±5 ‰ (Fig. 1B). The uncertainties in the LCIE factor were relatively higher than that of

208 the EIE factor, mainly because of the accumulated analytical uncertainties at low NO_x and O_3

209 concentrations, and low A values (0.10-0.28) due to the relatively low $j(NO_2)$ value (1.4×10^{-3} s^{-1})

210 under the chamber irradiation conditions.

211 We propose that our equations can be applied in the ambient environment to calculate the

212 combined isotopic fractionations of EIE and LCIE between NO and NO_2. First, the NO_2 sinks

213 (mainly NO_2+OH in the daytime) were at least 2-3 orders of magnitude slower than the Leighton

214 Cycle and the NO-NO_2 isotopic exchange (Walters et al., 2016), therefore their effects on the

215 $\delta(NO_2)$ should be insignificant. Second, although the conversion of NO to NO_2 in the ambient

216 environment is also controlled by NO + RO_2 and HO_2 in addition to NO+O_3, Eq. (7) still showed

217 good agreement with field observations in previous studies, suggesting the NO+RO_2/HO_2

218 reactions might have similar fractionation factors as NO+O_3. Freyer et al. (1993) measured the

219 annual average daytime $\delta(NO_2)$-$\delta(NO)$ at Julich, Germany along with average daytime NO

220 concentration (9 nmol mol^{-1}, similar to our experimental conditions) to be +18.03±0.98 ‰. Using

221 Eq. (7), assuming the daytime average $j(NO_2)$ value throughout the year was $5.0\pm1.0\times10^{-3}$, and a

222 calculated A value from measured NO_x concentration ranged from 0.22-0.33, the average NO-NO_2

223 fractionation factor was calculated to be +18.8±1.4 ‰ (Fig. 1B), in excellent agreement with the

224 measurements in the present study. Therefore, in the following discussion we will use this

Atmospheric
Chemistry
and Physics
Discussions

225   laboratory determined LCIE factor (-10 ‰) to calculate the nitrogen isotopic fractionation between

226   NO and NO_2 at various atmospheric conditions.

227   **3.3 Calculating nitrogen isotopic fractionations of NO-NO_2**

228   We first used Eq. (7) to calculate the NO-NO_2 isotopic fractionations ($\delta(NO_2)$-$\delta(NO)$) at a

229   wide range of NO_x concentrations, $f(NO_2)$ and $j(NO_2)$ values (Fig. 2A-D). $j(NO_2)$ values of 0 (Fig.

230   2A), 1.4×10^{-3} (Fig. 2B), 5×10^{-3} (Fig. 2C) and 1×10^{-2} (Fig. 2D) were selected to represent nighttime,

231   dawn (as well as the laboratory conditions of our experiments), daytime average and noon,

232   respectively. Each panel represented a fixed $j(NO_2)$ value, and the $\delta(NO_2)$-$\delta(NO)$ were calculated

233   as a function of the A value, which was derived from NO_x concentration and f_{NO2}. The A values

234   have a large span, from 0 to 500, depending on the $j(NO_2)$ value and the NO concentration. When

235   A=0 ($j(NO_2)$=0) and $f(NO_2)$<1 (meaning NO-NO_2 coexist and $[O_3]$=0), Eq. (7) and (8) become Eq.

236   (2) and (3), showing the EIE was the sole factor, the $\delta(NO_2)$-$\delta(NO)$ values were solely controlled

237   by EIE which has a constant value of +27.5 ‰ (Fig. 2A). When $j(NO_2)$ >0, the calculated $\delta(NO_2)$-

238    $\delta(NO)$ values showed a wide range from -10.0 ‰ (controlled by LCIE factor: α_2-α_1=-10 ‰) to

239   +27.5 ‰ (controlled by EIE factor: $\alpha(NO_2-NO)$-1=+27.5 ‰). Fig. 2B-D display the transition

240   from a LCIE-dominated regime to an EIE-dominated regime. The LCIE-dominated regime is

241   characterized by low $[NO_x]$ (<50 pmol mol^{-1}), representing remote ocean areas and polar regions

242   (Beine et al., 2002; Custard et al., 2015). At this range the A value can be greater than 200, thus

243   Eq. (7) can be simplified as: $\delta(NO_2)$-$\delta(NO)$=$(\alpha_2$-$\alpha_1) \times 1000$ ‰, suggesting the LCIE almost

244   exclusively controls the NO-NO_2 isotopic fractionation. The $\delta(NO_2)$-$\delta(NO)$ values of these regions

245   are predicted to be <0 ‰ during most time of the day and <-5 ‰ at noon. On the other hand, the

246   EIE-dominated regime was characterized by high $[NO_x]$ (>20 nmol mol^{-1}) and low $f(NO_2)$ (<0.6),

247   representative of regions with intensive NO emissions, e.g., roadside (Clapp & Jenkin, 2001;

248   Kimbrough et al., 2017). In this case, the $\tau_{exchange}$ are relatively short (10-50 s) compared to the

249   τ_{photo} (approximately 100 s at noon and 1000 s at dawn), therefore the A values are small (0.01-

250   0.5). The EIE factor in this regime thus is much more important than the LCIE factor, resulting in

251   high $\delta(NO_2)$-$\delta(NO)$ values (>20 ‰). Between the two regimes, both EIE and LCIE are competitive

252   and therefore it is necessary to use Eq. (7) to quantify the $\delta(NO_2)$-$\delta(NO)$ values.

253   Fig. 2 also implies that changes in the $j(NO_2)$ value may cause the diurnal variations in

254    $\delta(NO_2)$-$\delta(NO)$ and $\delta(NO_2)$-$\delta(NO_x)$ values. Changing $j(NO_2)$ would affect the value of A (Eq. (4)),

255   consequently the NO-NO$_2$ isotopic fractionations in two ways: 1) changes in $j(NO_2)$ value would

256   change the photolysis intensity, therefore the τ_{photo} value; 2) in addition, changes in $j(NO_2)$ value

257   would also alter the steady state NO concentration, therefore changing the $\tau_{exchange}$ (Fig. 2C). The

258   combined effect of these two factors on the A value varies along with the atmospheric conditions,

259   and thus needs to be carefully calculated using NO$_x$ concentration data and/or atmospheric

260   chemistry models.

261   We then calculated the differences of $\delta^{15}N$ values between NO$_2$ and NO$_x$ emissions

262   ($\delta(NO_2)$-$\delta(NO_x)$, Fig. 2E-H). Since $\delta(NO_2)$-$\delta(NO_x)$ are connected through the observed $\delta^{15}N$ of

263   NO$_2$ (or nitrate) to the $\delta^{15}N$ of NO$_x$ emissions, this term might be useful in field studies (e.g.,

264   Chang et al., 2018; Zong et al., 2017). The calculated $\delta(NO_2)$-$\delta(NO_x)$ values (Fig. 2E-H) also

265   showed a LCIE-dominated regime at low [NO$_x$] and an EIE-dominated regime at high [NO$_x$]. The

266    $\delta(NO_2)$-$\delta(NO_x)$ values were dampened by the 1-$f(NO_2)$ factor comparing to $\delta(NO_2)$-$\delta(NO)$, as

267   shown in Eq. (3) and (8): $\delta(NO_2)$-$\delta(NO_x)$=($\delta(NO_2)$-$\delta(NO)$)×(1-$f(NO_2)$). At high $f(NO_2)$ values

268   (>0.8), the differences between $\delta(NO_2)$ and $\delta(NO_x)$ were less than 5 ‰, thus the measured $\delta(NO_2)$

269   values were similar to $\delta(NO_x)$, although the isotopic fractionation between NO and NO$_2$ could be

270   noteworthy. Some ambient environments with significant NO emissions or high NO$_2$ photolysis

271   rates usually have $f(NO_2)$ values between 0.4-0.8 (Mazzeo et al., 2005; Vicars et al., 2013). In this

272   scenario, the $\delta(NO_2)$-$\delta(NO_x)$ values in Fig. 2F-H showed wide ranges of -4.8 ‰ to +15.6 ‰, -6.0 ‰

273   to +15.0 ‰, and -6.3 ‰ to +14.2 ‰ at $j(NO_2)=1.4\times10^{-3}$ s^{-1}, 5×10^{-3} s^{-1}, 1×10^{-2} s^{-1}, respectively.

274   These significant differences again highlighted the importance of both LCIE and EIE (Eq. (7) and

275   (8)) in calculating the $\delta(NO_2)$-$\delta(NO_x)$.

276

277   4. Implications

278   We first assessed the daily variation of $\delta(NO_2)$-$\delta(NO_x)$ values at two roadside NO_x

279   monitoring sites. Hourly NO and NO_2 concentrations was acquired from two sites at Anaheim, CA

280   (https://www.arb.ca.gov) and Evansville, IN (http://idem.tx.sutron.com) on July 25, 2018, then we

281   used $j(NO_2)$ values output from TUV model (Madronich & Flocke, 1999) at these locations to

282   calculate the daily variations of $\delta(NO_2)$-$\delta(NO_x)$ values (Fig. 3A, B) using Eq. (8). Hourly NO_x

283   concentrations were 12-51 nmol mol^{-1} at Anaheim and 9-38 nmol mol^{-1} at Evansville and the $f(NO_2)$

284   values at both sites did not show significant daily variations (0.45±0.07 at Anaheim and 0.65±0.08

285   at Evansville), likely because the NO_x concentrations were controlled by the high NO emissions

286   from the road (Gao, 2007). Assuming steady state isotopic fractionation was reached, the

287   calculated $\delta(NO_2)$-$\delta(NO_x)$ values showed significant diurnal variations. During the nighttime, the

288   isotopic fractionations were solely controlled by the EIE, the $\delta(NO_2)$-$\delta(NO_x)$ values were

289   +14.5±2.0 ‰ and +8.7±2.1 ‰ at Anaheim and Evansville, respectively. During the daytime, the

290   existence of LCIE lowered the $\delta(NO_2)$-$\delta(NO_x)$ values to +9.8±1.7 ‰ at Anaheim and +3.1±1.5 ‰

291   at Evansville while the $f(NO_2)$ values at both sites remained similar. The lowest $\delta(NO_2)$-$\delta(NO_x)$

292   values for both sites (+7.0 ‰ and +1.7 ‰) occurred around noon when the NO_x photolysis was

293   the most intense. In contrast, if one neglects the LCIE factor in the daytime, the $\delta(NO_2)$-$\delta(NO_x)$

294   values would be $+12.9\pm1.5$ ‰ and $+10.0\pm1.6$ ‰ respectively, an overestimation of 3.1 ‰ and

295   6.9 ‰. These discrepancies suggested that the LCIE played an important role in the NO-NO_2

296   isotopic fractionations and neglecting it could bias the NO_x source apportionment using $\delta^{15}N$ of

297   NO_2 or nitrate.

298   The role of LCIE was more important in less polluted sites. We calculated the $\delta(NO_2)$-

299    $\delta(NO_x)$ values (assuming steady state isotopic fractionation) at suburban San Diego, CA, USA,

300   again using the hourly NO_x concentrations (https://www.arb.ca.gov, Fig. 3C) and $j(NO_2)$ values

301   calculated from the TUV model. NO_x concentrations at this site varied from 1 to 9 nmol mol^{-1}.

302   During the nighttime, NO_x was in the form of NO_2 ($f(NO_2) = 1$) because O_3 concentrations were

303   higher than NO_x, thus the $\delta(NO_2)$ values should be identical to $\delta(NO_x)$. In the daytime a certain

304   amount of NO was produced by direct NO emission and NO_2 photolysis but the $f(NO_2)$ was still

305   high (0.73 ± 0.08). Our calculation suggested the daytime $\delta(NO_2)$-$\delta(NO_x)$ values should be only

306    $+1.3\pm3.2$ ‰ with a lowest value of -1.3 ‰. These $\delta(NO_2)$-$\delta(NO_x)$ values agree well with the

307   observed and modelled summer daytime $\delta(NO_2)$ values in West Lafayette, IN (Walters et al., 2018),

308   which suggest the average daytime $\delta(NO_2)$-$\delta(NO_x)$ values at $NO_x = 3.9\pm1.2$ nmol mol^{-1} should

309   range from +0.1 ‰ to +2.4 ‰. In this regime, we suggest the $\delta(NO_2)$-$\delta(NO_x)$ values were generally

310   small due to the significant contribution of LCIE and high $f(NO_2)$.

311   The LCIE should be the dominant factor controlling the NO-NO_2 isotopic fractionation at

312   remote regions, resulting in a completely different diurnal pattern of $\delta(NO_2)$-$\delta(NO_x)$ compared

313   with the urban-suburban area. Direct hourly measurements of NO_x at remote sites are rare, thus

314   we used total NO_x concentration of 50 pmol mol^{-1}, daily O_3 concentration of 20 nmol mol^{-1} at

315   Summit, Greenland (Dibb et al., 2002; Hastings et al., 2004; Honrath et al., 1999; Yang et al.,

316   2002), and assumed the conversion of NO to NO_2 was completely controlled by O_3 to calculate

317   the NO/NO$_2$ ratios. Here the isotopes of NO$_x$ were almost exclusively controlled by the LCIE due

318   to the high A values (>110). The δ(NO$_2$)-δ(NO$_x$) values displayed a clear diurnal pattern (Fig. 3D)

319   with highest value of -0.3 ‰ in the "nighttime" (solar zenith angle >85 degree) and lowest value

320   of -5.0 ‰ in the mid-day. This calculated daily variation of 4.7 ‰ was similar to the observed

321   δ^{15}N of nitrate (δ(NO$_3^-$)) in near-surface snow: Hastings et al. (2004) found that δ(NO$_3^-$) of samples

322   collected at early night (19:30) was 4-5 ‰ lower than those collected at early morning (07:00).

323   Since the nitrate samples were collected from the near surface, we suggest that the early night

324   samples should represent nitrate accumulated in the daytime, and the morning samples should

325   represent the nitrate formed in the "nighttime". This observation was in general agreement with

326   our prediction, indicating that the δ(NO$_2$) might played an important role in determining the

327   δ(NO$_3^-$). However, since the isotopic fractionation factors of nitrate-formation reactions (NO$_2$+OH,

328   NO$_3$+HC, N$_2$O$_5$+H$_2$O) are still unknown, more studies are needed to fully explain the daily and

329   seasonal variations of δ(NO$_3^-$) at remote regions.

330

331   **5. Conclusions**

332   We investigated the effect of NO$_x$ photochemistry on the nitrogen isotopic fractionations

333   between NO and NO$_2$. We first mathematically calculated the combined effects of EIE

334   (equilibrium isotopic fractionation caused by NO-NO$_2$ isotopic exchange) and LCIE (Leighton

335   Cycle induced isotopic fractionations) to demonstrate that the relative importance of EIE and LCIE

336   depends on NO, NO$_2$ concentrations and j(NO$_2$) value (Eq. (7) and Eq. (8)). We then measured the

337   isotopic fractionation factors of EIE and LCIE at room temperature to be 1.0275±0.0012 and

338   0.990±0.005, respectively. These calculations and measurements enabled us to calculate the steady

339   state δ(NO$_2$)-δ(NO)and δ(NO$_2$)-δ(NO$_x$)values at any given condition. Subsequently we applied

340   our equations to polluted, clean and remote sites to model the daily variations of $\delta(NO_2)$-$\delta(NO_x)$

341   values. We found that the $\delta(NO_2)$-$\delta(NO_x)$ values could vary from over +20 ‰ to less than -5 ‰

342   depending on the environment: in general, the role of LCIE becoming more important at low NO_x

343   concentrations, which tend to decrease the $\delta(NO_2)$-$\delta(NO_x)$ values. Our work provided a

344   mathematical approach to quantify the nitrogen isotopic fractionations between NO and NO_2 that

345   can be applied to many conditions, which could help interpret the measured $\delta^{15}N$ values of NO_2

346   and nitrate in field observation studies.

347

348   **Acknowledgement**

352   **Data Availability**

353   Data acquired from this study was deposited at Open Sciences Framework (Li, 2019,

354   DOI 10.17605/OSF.IO/JW8HU).

355   **Author contribution**

356   J. Li and G. Michalski designed the experiments, X. Zhang and J. Li conducted the

357   experiments. X. Zhang, G. Michalski, J. Orlando and G. Tyndall helped J. Li in interpreting the

358   results. The manuscript was written by J. Li and all the authors have contributed during the revision

359   of this manuscript.

360   **Competing interest**

361   The authors declare no competing interest.

362

References:

Atkinson, R., Baulch, D. L., Cox, R. A., Crowley, J. N., Hampson, R. F., Hynes, R. G., et al. (2004). Evaluated kinetic and photochemical data for atmospheric chemistry: Volume I-gas phase reactions of O_x, HO_x, NO_x and SO_x species. Atmospheric Chemistry and Physics, 4(6), 1461–1738.

Barney, W. S., & Finlayson-Pitts, B. J. (2000). Enhancement of N_2O_4 on porous glass at room temperature: A key intermediate in the heterogeneous hydrolysis of NO_2? The Journal of Physical Chemistry A, 104(2), 171–175.

Begun, G. M., & Fletcher, W. H. (1960). Partition function ratios for molecules containing nitrogen isotopes. The Journal of Chemical Physics, 33(4), 1083–1085.

Begun, G. M., & Melton, C. E. (1956). Nitrogen isotopic fractionation between NO and NO_2 and mass discrimination in mass analysis of NO_2. The Journal of Chemical Physics, 25(6), 1292–1293.

Beine, H. J., Honrath, R. E., Dominé, F., Simpson, W. R., & Fuentes, J. D. (2002). NO_x during background and ozone depletion periods at Alert: Fluxes above the snow surface. Journal of Geophysical Research: Atmospheres, 107(D21), ACH-7.

Bigeleisen, J., & Wolfsberg, M. (1957). Theoretical and experimental aspects of isotope effects in chemical kinetics. Advances in Chemical Physics, 15–76.

Casciotti, K. L., & McIlvin, M. R. (2007). Isotopic analyses of nitrate and nitrite from reference mixtures and application to Eastern Tropical North Pacific waters. Marine Chemistry, 107(2), 184–201.

Chang, Y., Zhang, Y., Tian, C., Zhang, S., Ma, X., Cao, F., et al. (2018). Nitrogen isotope fractionation during gas-to-particle conversion of NO_x to NO_3^- in the atmosphere–implications for isotope-based NO_x source apportionment. Atmospheric Chemistry and Physics, 18(16), 11647–11661.

Clapp, L. J., & Jenkin, M. E. (2001). Analysis of the relationship between ambient levels of O_3, NO_2 and NO as a function of NO_x in the UK. Atmospheric Environment, 35(36), 6391–6405.

Custard, K. D., Thompson, C. R., Pratt, K. A., Shepson, P. B., Liao, J., Huey, L. G., et al. (2015). The NO_x dependence of bromine chemistry in the Arctic atmospheric boundary layer. Atmospheric Chemistry and Physics, 15(18), 10799–10809.

Dibb, J. E., Arsenault, M., Peterson, M. C., & Honrath, R. E. (2002). Fast nitrogen oxide photochemistry in Summit, Greenland snow. Atmospheric Environment, 36(15–16), 2501–2511.

Elliott, E. M., Kendall, C., Boyer, E. W., Burns, D. A., Lear, G. G., Golden, H. E., et al. (2009). Dual nitrate isotopes in dry deposition: Utility for partitioning NO_x source contributions to landscape nitrogen deposition. Journal of Geophysical Research: Biogeosciences, 114(G4), G04020. https://doi.org/10.1029/2008JG000889

Felix, J. D., & Elliott, E. M. (2014). Isotopic composition of passively collected nitrogen dioxide emissions: Vehicle, soil and livestock source signatures. Atmospheric Environment, 92, 359–366.

Felix, J. D., Elliott, E. M., & Shaw, S. L. (2012). Nitrogen isotopic composition of coal-fired power plant NO_x: influence of emission controls and implications for global emission inventories. Environmental Science & Technology, 46(6), 3528–3535.

Freyer, H. D. (1991). Seasonal variation of $^{15}N/^{14}N$ ratios in atmospheric nitrate species. Tellus B, 43(1), 30–44. https://doi.org/10.1034/j.1600-0889.1991.00003.x

Freyer, H. D., Kley, D., Volz-Thomas, A., & Kobel, K. (1993). On the interaction of isotopic exchange processes with photochemical reactions in atmospheric oxides of nitrogen. Journal of Geophysical Research: Atmospheres, 98(D8), 14791–14796.

408 Gao, H. O. (2007). Day of week effects on diurnal ozone/NO_x cycles and transportation emissions
409 in Southern California. Transportation Research Part D: Transport and Environment, 12(4), 292–
410 305.
411 Gobel, A. R., Altieri, K. E., Peters, A. J., Hastings, M. G., & Sigman, D. M. (2013). Insights into
412 anthropogenic nitrogen deposition to the North Atlantic investigated using the isotopic
413 composition of aerosol and rainwater nitrate. Geophysical Research Letters, 40(22), 5977–5982.
414 https://doi.org/10.1002/2013GL058167
415 Hastings, M G, Jarvis, J. C., & Steig, E. J. (2009). Anthropogenic impacts on nitrogen isotopes of
416 ice-core nitrate. Science, 324(5932), 1288.
417 Hastings, M G, Steig, E. J., & Sigman, D. M. (2004). Seasonal variations in N and O isotopes of
418 nitrate in snow at Summit, Greenland: Implications for the study of nitrate in snow and ice cores.
419 Journal of Geophysical Research: Atmospheres, 109(D20).
420 Hoefs, J. (2009). Stable isotope geochemistry (Vol. 285). Springer.
421 Honrath, R. E., Peterson, M. C., Guo, S., Dibb, J. E., Shepson, P. B., & Campbell, B. (1999).
422 Evidence of NO_x production within or upon ice particles in the Greenland snowpack. Geophysical
423 Research Letters, 26(6), 695–698.
424 Jarvis, J. C., Steig, E. J., Hastings, M. G., & Kunasek, S. A. (2008). Influence of local
425 photochemistry on isotopes of nitrate in Greenland snow. Geophysical Research Letters, 35(21).
426 Kendall, C., Elliott, E. M., & Wankel, S. D. (2007). Tracing anthropogenic inputs of nitrogen to
427 ecosystems. Stable Isotopes in Ecology and Environmental Science, 2, 375–449.
428 Kimbrough, S., Owen, R. C., Snyder, M., & Richmond-Bryant, J. (2017). NO to NO_2 conversion
429 rate analysis and implications for dispersion model chemistry methods using Las Vegas, Nevada
430 near-road field measurements. Atmospheric Environment, 165, 23–34.
431 Li, J. (2019). Quantifying the nitrogen equilibrium and photochemistry-induced kinetic isotopic
432 effects between NO and NO_2. Retrieved from osf.io/jw8hu
433 Madronich, S., & Flocke, S. (1999). The role of solar radiation in atmospheric chemistry. In
434 Environmental photochemistry (pp. 1–26). Springer.
435 Mazzeo, N. A., Venegas, L. E., & Choren, H. (2005). Analysis of NO, NO_2, O_3 and NO_x
436 concentrations measured at a green area of Buenos Aires City during wintertime. Atmospheric
437 Environment, 39(17), 3055–3068.
438 McIlvin, M. R., & Altabet, M. A. (2005). Chemical conversion of nitrate and nitrite to nitrous
439 oxide for nitrogen and oxygen isotopic analysis in freshwater and seawater. Analytical Chemistry,
440 77(17), 5589–5595.
441 Michalski, G., Jost, R., Sugny, D., Joyeux, M., & Thiemens, M. (2004). Dissociation energies of
442 six NO_2 isotopologues by laser induced fluorescence spectroscopy and zero-point energy of some
443 triatomic molecules. The Journal of Chemical Physics, 121(15), 7153–7161.
444 Michalski, G., Bockheim, J. G., Kendall, C., & Thiemens, M. (2005). Isotopic composition of
445 Antarctic Dry Valley nitrate: Implications for NO_y sources and cycling in Antarctica. Geophysical
446 Research Letters, 32(13).
447 Miller, C. E., & Yung, Y. L. (2000). Photo-induced isotopic fractionation. Journal of Geophysical
448 Research: Atmospheres, 105(D23), 29039–29051.
449 Monse, E. U., Spindel, W., & Stern, M. J. (1969). Analysis of isotope-effect calculations illustrated
450 with exchange equilibria among oxynitrogen compounds. Rutgers-The State Univ., Newark, NJ.
451 Morin, S., Savarino, J., Frey, M. M., Domine, F., Jacobi, H.-W., Kaleschke, L., & Martins, J. M.
452 F. (2009). Comprehensive isotopic composition of atmospheric nitrate in the Atlantic Ocean
453 boundary layer from 65°S to 79°N. J. Geophys. Res, 114. https://doi.org/10.1029/2008JD010696

Atmospheric
Chemistry
and Physics
Discussions

454   Park, Y.-M., Park, K.-S., Kim, H., Yu, S.-M., Noh, S., Kim, M.-S., et al. (2018). Characterizing
455   isotopic compositions of TC-C, NO$_3^-$-N, and NH$_4^+$-N in PM2.5 in South Korea: Impact of China's
456   winter heating. https://doi.org/10.1016/j.envpol.2017.10.072
457   Do Remus, R. H., Mehrotra, Y., Lanford, W. A., & Burman, C. (1983). Reaction of water with
458   glass: influence of a transformed surface layer. Journal of Materials Science, 18(2), 612–622.
459   Saliba, N. A., Yang, H., & Finlayson-Pitts, B. J. (2001). Reaction of gaseous nitric oxide with
460   nitric acid on silica surfaces in the presence of water at room temperature. The Journal of Physical
461   Chemistry A, 105(45), 10339–10346.
462   Savarino, J., Morin, S., Erbland, J., Grannec, F., Patey, M. D., Vicars, W., et al. (2013). Isotopic
463   composition of atmospheric nitrate in a tropical marine boundary layer. Proceedings of the
464   National Academy of Sciences, 110(44), 17668–17673. https://doi.org/10.1073/pnas.1216639110
465   Sharma, H. D., Jervis, R. E., & Wong, K. Y. (1970). Isotopic exchange reactions in nitrogen oxides.
466   The Journal of Physical Chemistry, 74(4), 923–933.
467   Takei, T., Yamazaki, A., Watanabe, T., & Chikazawa, M. (1997). Water adsorption properties on
468   porous silica glass surface modified by trimethylsilyl groups. Journal of Colloid and Interface
469   Science, 188(2), 409–414.
470   Vicars, W. C., Morin, S., Savarino, J., Wagner, N. L., Erbland, J., Vince, E., et al. (2013). Spatial
471   and diurnal variability in reactive nitrogen oxide chemistry as reflected in the isotopic composition
472   of atmospheric nitrate: Results from the CalNex 2010 field study. Journal of Geophysical Research:
473   Atmospheres, 118(18), 10–567.
474   Walters, W. W., & Michalski, G. (2015). Theoretical calculation of nitrogen isotope equilibrium
475   exchange fractionation factors for various NO$_y$ molecules. Geochimica et Cosmochimica Acta,
476   164, 284–297.
477   Walters, W. W., Goodwin, S. R., & Michalski, G. (2015). Nitrogen stable isotope composition
478   (δ^{15}N) of vehicle-emitted NO$_x$. Environmental Science & Technology, 49(4), 2278–2285.
479   Walters, W. W., Simonini, D. S., & Michalski, G. (2016). Nitrogen isotope exchange between NO
480   and NO$_2$ and its implications for δ^{15}N variations in tropospheric NO$_x$ and atmospheric nitrate.
481   Geophysical Research Letters, 43(1), 440–448.
482   Walters, W. W., Fang, H., & Michalski, G. (2018). Summertime diurnal variations in the isotopic
483   composition of atmospheric nitrogen dioxide at a small midwestern United States city.
484   Atmospheric Environment, 179, 1–11.
485   Yang, J., Honrath, R. E., Peterson, M. C., Dibb, J. E., Sumner, A. L., Shepson, P. B., et al. (2002).
486   Impacts of snowpack emissions on deduced levels of OH and peroxy radicals at Summit,
487   Greenland. Atmospheric Environment, 36(15–16), 2523–2534.
488   Zhang, X., Ortega, J., Huang, Y., Shertz, S., Tyndall, G. S., & Orlando, J. J. (2018). A steady-state
489   continuous flow chamber for the study of daytime and nighttime chemistry under atmospherically
490   relevant NO levels. Atmospheric Measurement Techniques, 11(5), 2537–2551.
491   Zong, Z., Wang, X., Tian, C., Chen, Y., Fang, Y., Zhang, F., et al. (2017). First assessment of NO$_x$
492   sources at a regional background site in North China using isotopic analysis linked with modeling.
493   Environmental Science & Technology, 51(11), 5923–5931.

Atmospheric
Chemistry
and Physics
Discussions

Open Access
EGU
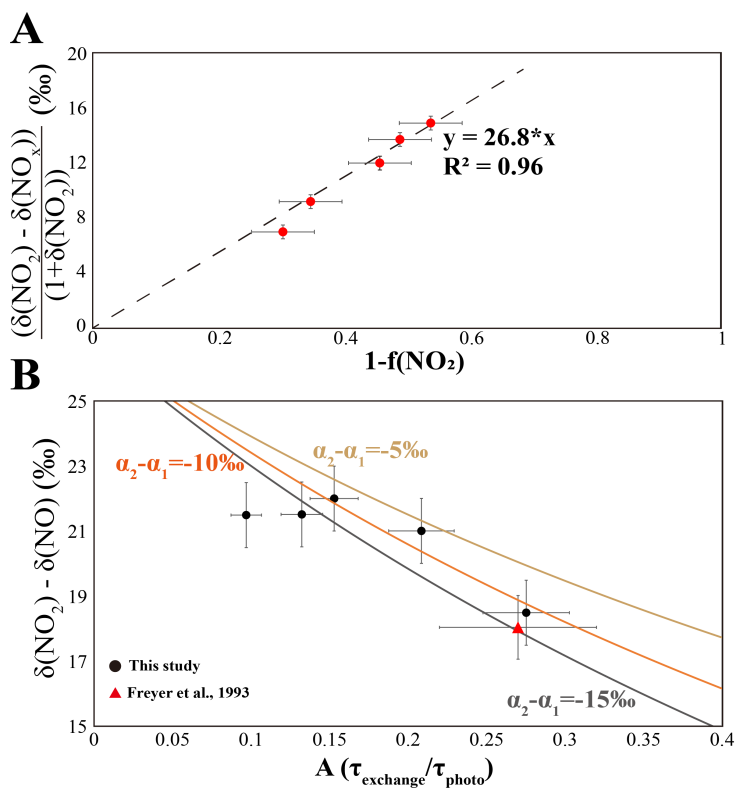
494
495
Fig. 1 $\delta^{15}N$ of NO_2 collected in dark and UV irradiation experiments. **A.** Results from five dark
experiments yielded a line with $\varepsilon(NO_2\text{-}NO)/(1+\varepsilon(NO_2\text{-}NO))$ value of 26.8 ‰ and $\varepsilon(NO_2\text{-}NO)$
value of 27.5 ‰; **B.** Results from five UV irradiation experiments (black points) and a previous
field study (red triangle). The three lines represent different $(\alpha_2\text{-}\alpha_1)$ values: the $(\alpha_2\text{-}\alpha_1)$=-10 ‰ line
showed the best fit to our experimental data as well as the previous field observation.
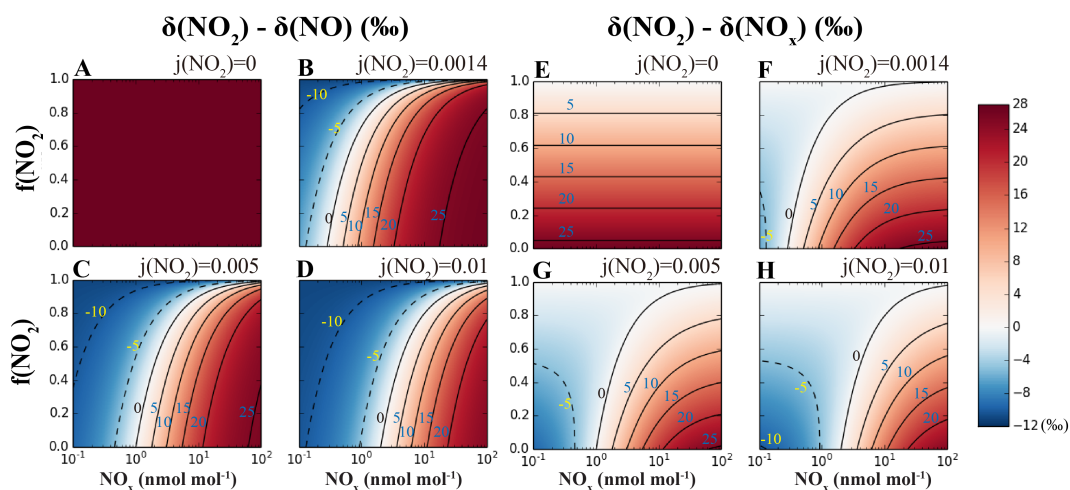
Fig. 2 Calculating isotopic fractionation values between NO-NO$_2$ (δ(NO$_2$)-δ(NO), **A-D**) and NO$_x$-NO$_2$ (δ(NO$_2$)-δ(NO$_x$), **E-H**) at various j(NO$_2$), NO$_x$ level and f(NO$_2$) using Eq. (7) and (8). Each panel represents a fixed j value (showing on the upper right side of each panel), and the fractionation values are shown by color. Lines are contours with constant fractionation values and each number on the contour represents its value.

508
509
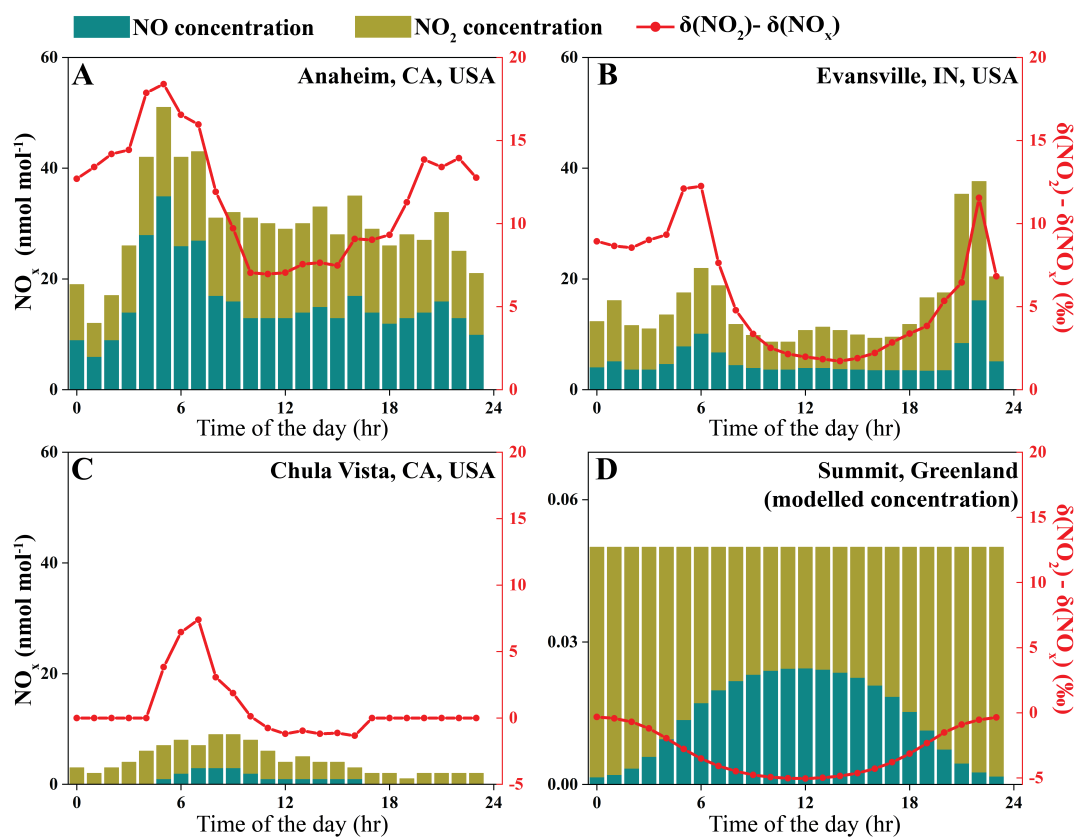
Fig. 3 NO_x concentrations and calculated $\delta(NO_2)$-$\delta(NO_x)$ values at four sites. Stacked bars show
the NO and NO_2 concentrations extracted from monitoring sites (A-C) or calculated using 0-D box
model (D); the red lines are $\delta(NO_2)$-$\delta(NO_x)$ values at each site.